The International Journal of Advanced Manufacturing Technology (2024) 134:2051–2065
https://doi.org/10.1007/s00170-024-14141-2

ORIGINAL ARTICLE

A novel methodology for the selection of the optimal velocity profile for planned point-to-point trajectories in 1-DoF manipulators

Camilo Andrés Gonzalez Olier[1] · **Heriberto Enrique Maury Ramírez**[2] · **Leidy Milena Mora Higuera**[3]

Received: 17 April 2024 / Accepted: 12 July 2024 / Published online: 14 August 2024

Abstract

In this work, an approach based on velocity profile selection is developed and validated to decrease forces, acceleration, velocity, mechanical power, and energy consumption in 1 DOF Cartesian manipulators. Initially, a mathematical modeling of the kinematic and kinetic variables rising in linear, exponential, parabolic, sinusoidal, and s-curve ramp *velocity* profiles is proposed for different load conditions and saturation values of the velocity profiles, focusing on generic Cartesian manipulators moving a constant inertia load and not equipped with regenerative devices. Lastly, a summary table outlining the benefits and drawbacks of each velocity profile in relation to the relevant variables is given to the reader, along with a set of recommendations for selecting the best velocity profile in accordance with the load conditions and optimization goals. It was shown that, depending on the load conditions, the inappropriate choice of one type of speed profile can increase the required forces by up to 400%, the required maximum power by more than 88%, and the energy consumption by up to 77% with respect to the optimal speed profile.

Keywords Energy saving · Cartesian manipulators · Velocity profile selection · Point-to-point motions · Trajectory planning

Nomenclature

a	Acceleration
a_Δ	Acceleration in triangular profile
E	Energy consumption
F	Total loads
F_I	Inertial loads
$F_{I\Delta}$	Inertial loads in triangular profile
F_{NI}	Non-inertial loads
m	Handled mass
P	Mechanical power
P_Δ	Mechanical power in triangular profile
$P_{i\Delta}$	Mechanical power in triangular profile associated with inertial loads
t	Time.
T	Total movement time.
T_a	Acceleration movement time
T_v	Movement time at constant velocity
V	Velocity
V_{max}	Velocity in triangular profile
V_Δ	Maximum velocity
δ	Displacement performed at constant speed
δ_{ad}	Sum of displacements during acceleration and deceleration.
δ_v	Displacement at constant velocity
ξ	Velocity profile saturation.
$\forall$	For all
$\in$	Is an element of
λ	Ratio between non-inertial forces and inertial loads in triangular velocity profile

✉ Camilo Andrés Gonzalez Olier
camilo.gonzalezo@unisimon.edu.co

Heriberto Enrique Maury Ramírez
hmaury@uninorte.edu.co

Leidy Milena Mora Higuera
l.mora@unireformada.edu.co

[1] Faculty of Engineering, Universidad Simon Bolivar, Barranquilla, Colombia

[2] Mechanical Engineering Department, Universidad del Norte, Puerto Colombia, Colombia

[3] Industrial Engineering Department, Corporación Universitaria Reformada, Barranquilla, Colombia

1 Introduction

The use of robotic manipulators for various activities is becoming increasingly common, being used in applications as diverse as agriculture [1, 2], manufacturing [3–8], and medicine [9, 10], among many others. The implementation of these manipulators allows operations to be carried out accurately and quickly, while reducing operating costs and preventing humans from performing potentially dangerous tasks [11–13].

One of the main tasks when using manipulators in such applications is the planning of their motion, which has been a recurring challenge in robotics [14, 15]. For control purposes, it is important to establish the velocity and acceleration profiles for every motion cycle of the manipulator when defining the motion between two points, where velocity profiles are understood as the equation of velocity as a function of time for the motion of a mechanical system. In the same way, the acceleration profile will be understood as the acceleration equation as a function of time for a given mechanical system. There are many types of velocity profiles as a function of time in the literature, such as linear [16–18], exponential, parabolic [19, 20], sinusoidal [21], and S-curve profiles [16, 22, 23], which characterize the velocity behavior of manipulators as a function of time.

The correct definition of the velocity profiles is crucial during the trajectories planning process because it will directly affect the costs and the environmental impact of the processes. Given that the kinematics have an impact on the forces, power, and energy consumption of the manipulators [24–26], analyses show, for example, case studies in which the energy consumption of a specific movement can be increased by 100% simply by decisions associated with the movement strategy to be followed in a particular trajectory [26]. That is why the objective of this work is to provide a methodology for the correct selection of velocity profiles to optimize manipulator performance, minimizing variables such as velocity, acceleration, jerk, forces, mechanical power, or energy consumption according to the design requirements.

The impact of velocity profiles on energy consumption has been studied by authors such as Zhu and Carabin [18, 20], whose studies suggest that it is possible to minimize the energy consumption of manipulators in point-to-point trajectories by the proper selection of velocity profiles, either by computational iteration or by modeling the dynamics of the system, with emphasis on trapezoidal and smooth curve profiles. However, their models require the selection of a motor in order to characterize the energy consumption of manipulators [11, 20] because they require parameters such as the electrical resistance constant of the motor, which is a constraint in the design process. Similar investigations study the optimization of consumption based on other factors, such as the appropriate selection of gear ratios between the engine and the mechanism [27–29], in which reductions in energy dissipation of more than 50% have been documented through the transmission ratio of the motor to the mechanical system when comparing these methods with older methods such as the inertia matching method.

The issue of jerk minimization has also been evaluated in similar studies [16, 21]; however, the inclusion of the saturation of velocity profiles (ξ), which is a relevant parameter since it determines what fraction of the movement time the system will move at constant velocity, has not been studied for profiles such as parabolic and exponential.

On the other hand, aspects such as the implications of the definition of velocity in mechanical power, forces, and kinematics have not been studied in depth in the literature for profiles other than linear [26].

Methodologies similar to those mentioned above consist of graphical methods, such as power transients, to validate that the drive systems can deliver power at the rate required by the mechanism during the transient regime [30–34].

This methodology is novel because it allows the designer to select a velocity profile to perform point-to-point trajectories in 1 degree of freedom (1-DOF) systems, minimizing velocities, accelerations, jerk, forces, power, or energy consumption according to their design needs based on simple guidelines without having to select elements of the drive system. Although the principles of this methodology are presented in a general way, it is only applicable to 1-DOF Cartesian manipulators because it does not consider the effect of the superposition of movements in several axes or the possible changes in inertia caused by the changes in orientation of the links that compose the mechanism, an effect that does occur in other types of manipulator structures.It is important to emphasize that the equations used to model this type of system are subject to various uncertainties, such as uncertainties in the dynamics of the system due to unmodeled dynamic effects, internal disturbances or external disturbances [35, 36]. Among these disturbances, we can mention friction subject to external parameters, such as temperature [37], Non-linear forces [37–39]. Although solutions to deal with this uncertainty, such as fuzzy logic or adaptive fuzzy, are mentioned in the literature, such strategies will not be addressed in this manuscript [36, 39–41].

2 Point-to-point industrial trajectory profiles

There are many types of profiles for point-to-point paths in the literature. These can be classified according to the type of ramp or according to the ratio between the constant speed

movement time and the total movement time. In this section, the basic parameters and classification of the speed profiles, will be described, which will then be evaluated taking into account the following performance indicators:

- Maximum velocity: This performance indicator is included because maximum speed is a typical constraint in cargo handling operations [17, 26, 34].
- Maximum acceleration: This performance indicator is included because the maximum acceleration is directly linked to the inertial forces and the intensity of the vibrations that will be reflected in the manipulator. [16, 21, 29]:
- Maximum force: This performance indicator is included because the maximum force exerted by the manipulator will influence the requirements on the mechanical drive, guidance, and support elements that make up the system.
- Maximum mechanical power: This performance indicator is included because it is associated with the power required by the drive [19, 26].
- Energy consumption: This performance indicator is included because it is associated with the operating costs and emissions associated with the operation of the manipulator [26]. Additionally, it is the most common indicator analysed in the literature [18–20].

2.1 Classification of velocity profiles according to ramp type

The motion of manipulators could be defined by the designer using a variety of velocity vs. time functions during acceleration phases. The graph of velocity vs. time during this acceleration period is known as a ramp [42].

If the rate of change of the velocity is constant, the velocity profile is said to have a linear ramp. These profiles are currently the most widely used due to their simplicity. For the point case where the velocity does not reach a constant value, profiles with linear ramps are known as triangular profiles, and for the case where the velocity reaches a constant value between acceleration and deceleration periods, profiles with linear ramps are known as trapezoidal profiles [16–18]. Linear velocity profiles are the most widely used due to their ease of calculation in the design of control systems [20, 30].

When the equation of the velocity as a function of time is given by an exponential relationship when accelerating and when decelerating, the profile is said to have an exponential ramp [29, 43]. These profiles have the advantage that they are easy to control since they can be generated from RC circuits; however, they result in higher accelerations than linear velocity profiles, which can lead to a reduction in the life of the drive and the coupled mechanical system.

Table 1 Velocity as a function of time according to the type of ramp of the velocity profile when periods of motion at constant velocity are not considered

Velocity profile ramp	Velocity function	
Linear	$V(t) = \begin{cases} \frac{2V_{max}t}{T} \\ \frac{2V_{max}(T-t)}{T} \end{cases}$	$\forall t \in \left[0, \frac{T}{2}\right)$ $\forall t \in \left[\frac{T}{2}, T\right]$
Exponential	$V(t) = \begin{cases} V_{max}\left(1 - e^{-\frac{10t}{T}}\right) \\ V_{max}e^{-\frac{5(2t-T)}{T}} \end{cases}$	$\forall t \in \left[0, \frac{T}{2}\right)$ $\forall t \in \left[\frac{T}{2}, T\right]$
Parabolic	$V(t) = \left\{ \frac{4V_{max}t}{T^2}(T-t) \right.$	$\forall t \in [0, T]$
Sinusoidal	$V(t) = \left\{ \frac{V_{max}}{2}\left(1 - \cos\left(\frac{2\pi t}{T}\right)\right) \right.$	$\forall t \in [0, T]$
S-Curve	$V(t) = \begin{cases} 4V_{max}\left(\frac{3}{T^2}t^2 - \frac{4}{T^3}t^3\right) \\ \frac{4V_{max}}{T^3}(T-t)^2(4t-T) \end{cases}$	$\forall t \in \left[0, \frac{T}{2}\right)$ $\forall t \in \left[\frac{T}{2}, T\right]$

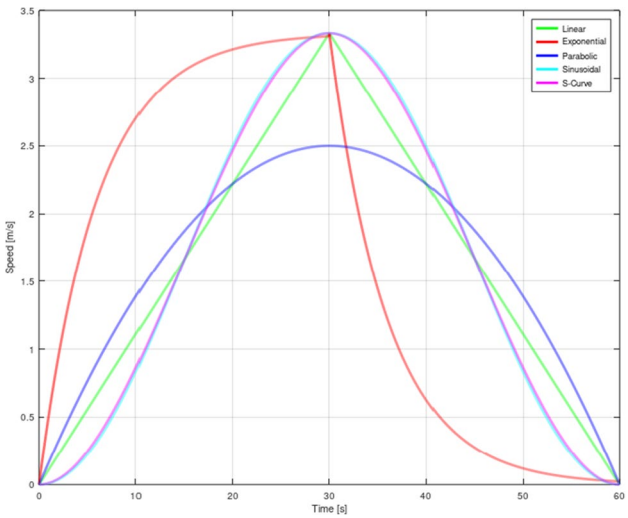

Fig. 1 Velocity profiles with different types of ramps taking as reference a displacement of 100 m performed in a time of 60 s

Linear and exponential profiles are inconvenient from the vibration point of view because they cause undesired jerk values. This drawback can be solved by using profiles with smooth curves [21, 44, 45]. The most commonly used soft curve profiles are parabolic profiles [19], sinusoidal profiles [20, 21], and s-curve profiles [22, 46, 47].

The equations of the velocity profiles when periods of movement with constant velocity are not contemplated are shown in Table 1. Figure 1 shows the behavior of the velocity as a function of time for different ramp times, taking as a reference a displacement of 100 m performed in a time of 60 s, assuming that the displacement is performed with an acceleration stage and a deceleration stage.

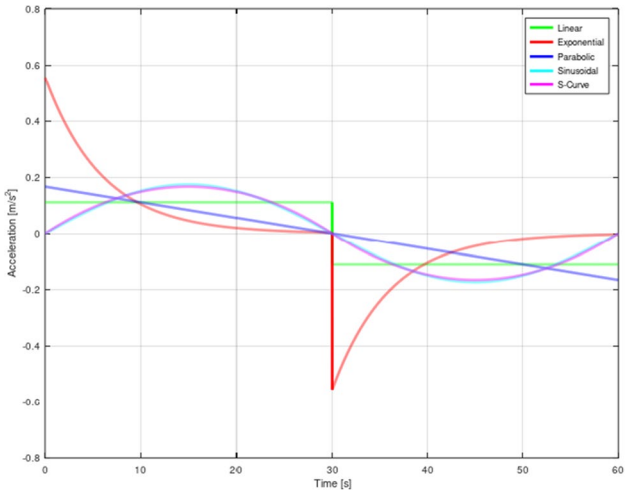

Fig. 2 Acceleration profiles with different types of ramps taking as reference a displacement of 100 m performed in a time of 60 s

When comparing the sinusoidal profile and the s-curve profile, no significant differences were observed. This is due to the fact that when the percentage difference between the velocities of these profiles is less than 15% for any instant of time, this difference is much smaller when the velocities approach their maximum value (for example, in the time interval, the difference is less than 2%). This conclusion can be obtained numerically from the velocity equations as a function of time shown in Table 1.

Acceleration profiles can be obtained from the derivatives with respect to the time of the velocity functions. The acceleration profiles for each of the ramps are shown in Fig. 2. As can be seen in Fig. 2, the lowest maximum acceleration is obtained when using linear velocity profiles, and the highest accelerations are obtained when using exponential velocity profiles. Additionally, the acceleration profiles in the linear and exponential profiles have discontinuities, which implies that at these points, the jerk will theoretically tend to infinity, causing vibration problems.

The parabolic, sinusoidal, and s-curve profiles do not present discontinuities in the acceleration vs. time curve; the sinusoidal and s-curve profiles are the ones that present the lowest jerk values due to their smooth transition compared to the parabolic profiles.

2.2 Saturation of velocity profiles (ξ)

In Table 1, the equations assume that the periods into which the cycle is divided are only one acceleration and one deceleration stage. However, depending on the kinematic constraints, it is possible to realize trajectories in which, between the acceleration and deceleration periods, there is a period of time in which the motion is performed at constant velocity.

The proportion of time in which the drive moves at constant velocity divided by the total movement time for a single cycle is known as the velocity profile saturation, or saturation (ξ) [26, 34], which can take values in the range ($0 \leq \xi < 1$). To illustrate the effect of saturation on velocity, and acceleration, a linear ramp profile will be used as a reference. In these profiles, the velocity and acceleration in terms of displacement, time, and saturation are given by the following equations [26]:

$$V(t) = \frac{2\delta}{(1+\xi)t} \tag{1}$$

$$a(t) = \frac{4\delta}{\left(1-\xi^2\right)t^2} \tag{2}$$

The effect of saturation on the velocity and acceleration profiles is shown in Figs. Figure 3 and Fig. 4. As can be seen, velocity is inversely proportional to saturation, while acceleration is proportional to saturation.

3 Velocity and acceleration modeling

The first step to be carried out is to derive general expressions for the velocity profiles. For this purpose, the total displacement and the velocity function in terms of time are related by means of Eq. (1).

$$\int_0^T V(t)dt = \delta \tag{1}$$

Generally, it will be assumed that there are 3 stages of motion: an initial accelerating stage, a constant velocity stage, and a decelerating stage (whose duration is assumed to be

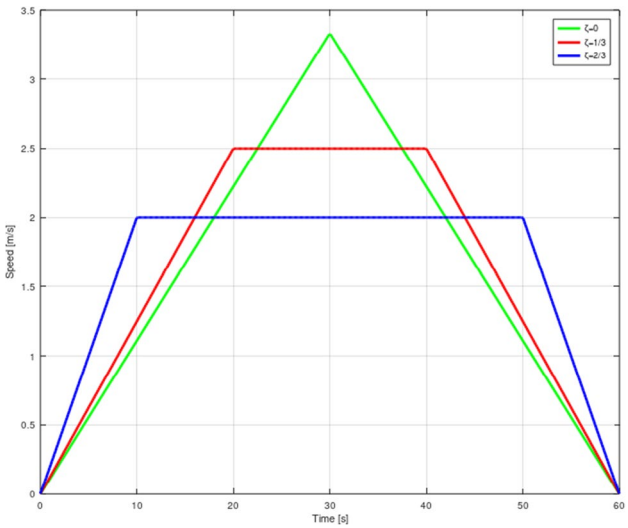

Fig. 3 Velocity profiles with different types of cuspids taking as reference a displacement of 100 m performed in a time of 60 s

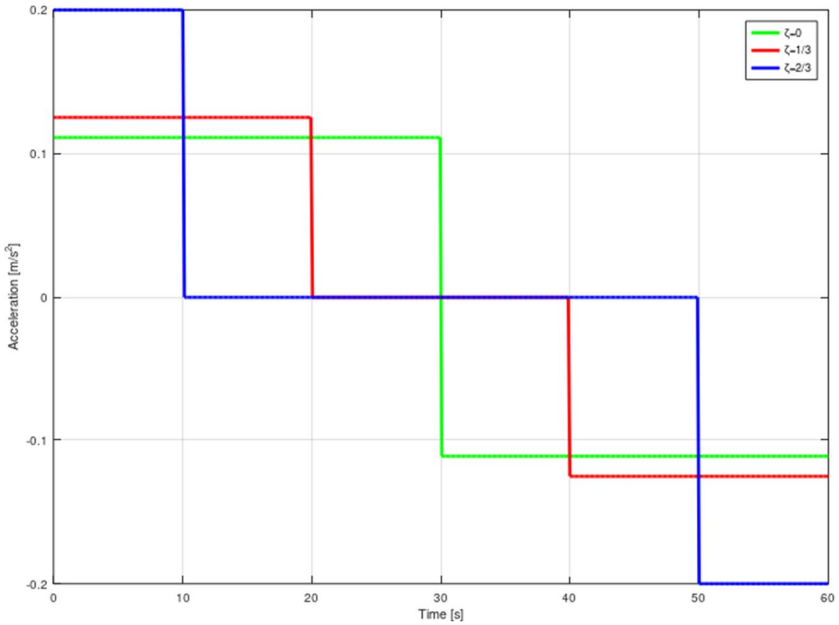

Fig. 4 Acceleration profiles with different types of cuspids taking as reference a displacement of 100 m performed in a time of 60 s

equal to that of the acceleration time). Considering that saturation (ζ) is defined as the ratio between the time of motion at constant velocity and the total time in one cycle, the durations of the acceleration (T_a) and motion at constant velocity (T_v) times are given by the Eqs. (4) – (5).

$$T_v = T\zeta \tag{4}$$

$$T_a = \frac{T(1-\zeta)}{2} \tag{5}$$

The displacement realized in the constant velocity cycle is equal to the maximum velocity multiplied by the time of this cycle, while the displacement realized during the transient period (including acceleration and deceleration) is a function of the maximum velocity of the cycle, the type of profile, and the acceleration time. To better exemplify this premise, the formula for maximum velocity in the parabolic profile of Table 1 will be taken as an example. Considering Eqs. (1) and (3), the following relationship between the displacement during the transient period and the maximum velocity can be obtained:

$$\delta_{ad} = \frac{2V_{max}T(1-\zeta)}{3} \tag{6}$$

Therefore, the maximum velocity formula (Eq. 8) can be derived in terms of time, displacement, and saturation from Eq. 5:

$$\delta_v + \delta_{ad} = \delta \tag{7}$$

$$\frac{2V_{max}T(1-\zeta)}{3} + V_{max}T\zeta = \delta \rightarrow V_{max} = \frac{3\delta}{T(2+\zeta)} \tag{8}$$

Taking as a reference the maximum velocity in a triangular profile V_Δ, (when $\zeta = 0$) this formula can be rewritten as shown in Eq. 9.

$$V_{max} = V_\Delta\left(\frac{3}{2(2+\zeta)}\right) \tag{9}$$

Applying this analysis to the other velocity profiles, it is concluded that, with the exception of the quadratic velocity profile, all the profiles satisfy Eq. 10:

$$V_{max} = \frac{2\delta}{T(1+\zeta)} = \frac{V_\Delta}{(1+\zeta)} \tag{10}$$

The maximum velocities achieved for each velocity profile as a function of saturation are shown in Fig. 5. The

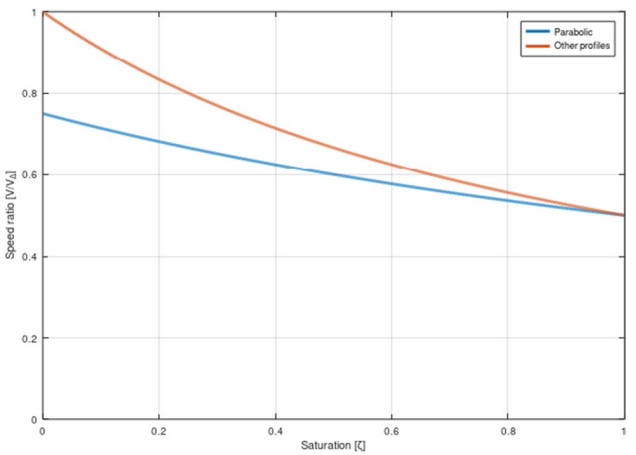

Fig. 5 Ratio of maximum velocity to triangular maximum velocity

Table 2 Velocity as a function of dimensionless time (τ) for various types of profiles

Velocity profile ramp	Velocity function	
Linear	$V(\tau)=\begin{cases}\frac{2V_\Delta\tau}{(1-\zeta^2)}\\ \frac{V_\Delta}{(1+\zeta)}\\ \frac{2V_\Delta(1-\tau)}{(1-\zeta^2)}\end{cases}$	$\begin{matrix}\forall\tau\in\left[0,\frac{(1-\zeta)}{2}\right)\\ \forall\tau\in\left[\frac{(1-\zeta)}{2},\frac{(1+\zeta)}{2}\right)\\ \forall\tau\in\left[\frac{(1-\zeta)}{2},1\right]\end{matrix}$
Exponential	$V(\tau)=\begin{cases}\frac{V_\Delta}{(1+\zeta)}\left(1-e^{-\frac{10\tau}{(1-\zeta)}}\right)\\ \frac{V_\Delta}{(1+\zeta)}\\ \frac{V_\Delta}{(1+\zeta)}e^{-\frac{5(2\tau-(1+\zeta))}{(1-\zeta)}}\end{cases}$	$\begin{matrix}\forall\tau\in\left[0,\frac{(1-\zeta)}{2}\right)\\ \forall\tau\in\left[\frac{(1-\zeta)}{2},\frac{(1+\zeta)}{2}\right)\\ \forall\tau\in\left[\frac{(1-\zeta)}{2},1\right]\end{matrix}$
Parabolic	$V(\tau)=\begin{cases}\frac{6V_\Delta\tau((1-\zeta)-\tau)}{(1-\zeta)^2(2+\zeta)}\\ V_\Delta\left(\frac{3}{2(2+\zeta)}\right)\\ \frac{6V_\Delta(\tau-\zeta)((1-\zeta)-(\tau-\zeta))}{(1-\zeta)^2(2+\zeta)}\end{cases}$	$\begin{matrix}\forall\tau\in\left[0,\frac{(1-\zeta)}{2}\right)\\ \forall\tau\in\left[\frac{(1-\zeta)}{2},\frac{(1+\zeta)}{2}\right)\\ \forall\tau\in\left[\frac{(1-\zeta)}{2},1\right]\end{matrix}$
Sinusoidal	$V(\tau)=\begin{cases}\frac{V_\Delta}{2(1+\zeta)}\left(1-\cos\left(\frac{2\pi\tau}{(1-\zeta)}\right)\right)\\ \frac{V_\Delta}{(1+\zeta)}\\ \frac{V_\Delta}{2(1+\zeta)}\left(1-\cos\left(\frac{2\pi(\tau-\zeta)}{(1-\zeta)}\right)\right)\end{cases}$	$\begin{matrix}\forall\tau\in\left[0,\frac{(1-\zeta)}{2}\right)\\ \forall\tau\in\left[\frac{(1-\zeta)}{2},\frac{(1+\zeta)}{2}\right)\\ \forall\tau\in\left[\frac{(1-\zeta)}{2},1\right]\end{matrix}$
S-Curve	$V(\tau)=\begin{cases}\frac{4V_\Delta}{(1+\zeta)}\left(\frac{3\tau^2}{(1-\zeta)^2}-\frac{4\tau^3}{(1-\zeta)^3}\right)\\ \frac{V_\Delta}{(1+\zeta)}\\ \frac{4V_\Delta}{(1-\zeta)^3(1+\zeta)}(1-\tau)^2(4\tau-3\zeta-1)\end{cases}$	$\begin{matrix}\forall\tau\in\left[0,\frac{(1-\zeta)}{2}\right)\\ \forall\tau\in\left[\frac{(1-\zeta)}{2},\frac{(1+\zeta)}{2}\right)\\ \forall\tau\in\left[\frac{(1-\zeta)}{2},1\right]\end{matrix}$

equations the velocity as a function of dimensionless time $\tau=\left(\frac{t}{T}\right)$ are shown in Table 2.

The relationship between the maximum velocity in any given profile and the maximum velocity in a triangular profile (Eq. 10 when $\zeta=0$) as a function of saturation is shown in the Fig. 11.

The above allows observing that parabolic profiles allow obtaining equal displacements with lower velocities, allowing decreasing the maximum velocity up to 25%. Once the velocity profile functions have been derived, the acceleration profiles can be obtained based on the formal definition of acceleration described in Eq. 11:

$$a(t)=\frac{dV(t)}{dt} \tag{11}$$

According to the type of ramp of the velocity profiles, the times at which the maximum accelerations are obtained vary from one to another and do not necessarily coincide with the time at which the maximum velocity occurs. This information is shown in Table 3.

Based on Eq. 11 the acceleration equations in terms of dimensionless time are derived as shown in Table 4. Taking as a reference Eq. 10, it follows that the acceleration in a triangular profile is given by Eq. 12.

Table 3 Time at which the maximum acceleration is obtained depending on the type of ramp of the velocity profile

Velocity profile ramp	Time
Linear	$\forall t\in[0,T_a)$
Exponential	$t=0$
Parabolic	$t=0$
Sinusoidal	$t=\frac{T_a}{2}$
S-Curve	$t=\frac{T_a}{2}$

$$a_\Delta=\frac{4\delta}{T^2} \tag{12}$$

By evaluating the formulas of the acceleration profiles at this time, the ratio between the maximum acceleration (obtained from the equations in Table 4, evaluated at the maximum acceleration times established in Table 3) and the acceleration in a triangular profile (Eq. 12) was obtained in Fig. 6, where the behavior of the maximum acceleration as a function of saturation can be observed. It can be observed that, regardless of the saturation value, the minimum accelerations are obtained in profiles with linear ramps, while the maximum accelerations are obtained in profiles with exponential ramps.

Table 4 Acceleration as a function of dimensionless time (τ) for various types of profiles

Velocity profile ramp	Acceleration function
Linear	$a(\tau)=\begin{cases}\frac{a_\Delta}{(1-\zeta^2)} & \forall\tau\in\left[0,\frac{(1-\zeta)}{2}\right)\\ 0 & \forall\tau\in\left[\frac{(1-\zeta)}{2},\frac{(1+\zeta)}{2}\right)\\ \frac{-a_\Delta}{(1-\zeta^2)} & \forall\tau\in\left[\frac{(1-\zeta)}{2},1\right]\end{cases}$
Exponential	$a(\tau)=\begin{cases}\frac{5a_\Delta}{(1-\zeta^2)}e^{-\frac{10\tau}{(1-\zeta)}} & \forall\tau\in\left[0,\frac{(1-\zeta)}{2}\right)\\ 0 & \forall\tau\in\left[\frac{(1-\zeta)}{2},\frac{(1+\zeta)}{2}\right)\\ \frac{-5a_\Delta}{(1-\zeta^2)}e^{-\frac{5(2\tau-(1+\zeta))}{(1-\zeta)}} & \forall\tau\in\left[\frac{(1-\zeta)}{2},1\right]\end{cases}$
Parabolic	$a(\tau)=\begin{cases}\frac{3a_\Delta}{(1-\zeta)^2(2+\zeta)}[(1-\zeta)-2\tau] & \forall\tau\in\left[0,\frac{(1-\zeta)}{2}\right)\\ 0 & \forall\tau\in\left[\frac{(1-\zeta)}{2},\frac{(1+\zeta)}{2}\right)\\ \frac{3a_\Delta}{(1-\zeta)^2(2+\zeta)}[(1-\zeta)-2(\tau-\zeta)] & \forall\tau\in\left[\frac{(1-\zeta)}{2},1\right]\end{cases}$
Sinusoidal	$a(\tau)=\begin{cases}\frac{a_\Delta}{2(1-\zeta^2)}\left(\pi sen\left(\frac{2\pi\tau}{(1-\zeta)}\right)\right) & \forall\tau\in\left[0,\frac{(1-\zeta)}{2}\right)\\ 0 & \forall\tau\in\left[\frac{(1-\zeta)}{2},\frac{(1+\zeta)}{2}\right)\\ \frac{a_\Delta}{2(1-\zeta^2)}\left(\pi sen\left(\frac{2\pi(\tau-\zeta)}{(1-\zeta)}\right)\right) & \forall\tau\in\left[\frac{(1-\zeta)}{2},1\right]\end{cases}$
S-Curve	$a(\tau)=\begin{cases}\frac{12a_\Delta\tau}{(1+\zeta)}\left(\frac{(1-\zeta)-2\tau}{(1-\zeta)^3}\right) & \forall\tau\in\left[0,\frac{(1-\zeta)}{2}\right)\\ 0 & \forall\tau\in\left[\frac{(1-\zeta)}{2},\frac{(1+\zeta)}{2}\right)\\ \frac{12a_\Delta}{(1+\zeta)}\left(\frac{(1-\zeta)^2-3(1-\zeta)(\tau-\zeta)+2(\tau-\zeta)^2}{(1-\zeta)^3}\right) & \forall\tau\in\left[\frac{(1-\zeta)}{2},1\right]\end{cases}$

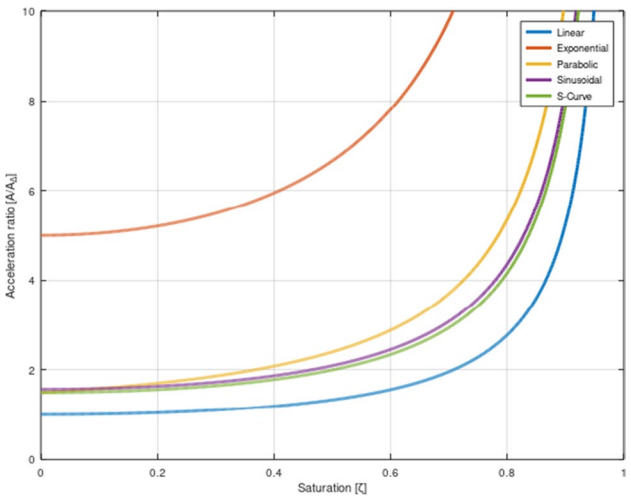

Fig. 6 Ratio of maximum acceleration to triangular acceleration

4 Force requirements modeling

The load required by a system is the sum of an inertial load component (F_I) and a non-inertial load component (F_{NI}). The non-inertial loads are independent of the manipulator kinematics, while the inertial loads are not, and are therefore influenced by the saturation value. The ratio between non-inertial loads and inertial loads in the triangular profile ($F_{I\Delta}$) is called λ [26], and is calculated based on Eq. 13.

$$\lambda=\frac{F_{NI}}{F_{I\Delta}}=\frac{F_{NI}}{ma_\Delta} \tag{13}$$

As can be seen in Table 4, the acceleration of a velocity profile can be calculated as shown in Eq. 14, where $f(\tau,\zeta)$ is a function that varies according to the type of ramp of the velocity profile:

$$a(\tau)=a_\Delta f(\tau,\zeta) \tag{14}$$

Considering Eqs. 13 and 14, Eq. 15 is obtained, where the total force is calculated.

$$F(\tau)=F_{NI}+F_I(\tau)=F_{NI}+ma_\Delta f(\tau,\zeta)=ma_\Delta(\lambda+f(\tau,\zeta)) \tag{15}$$

The maximum force in each velocity profile considering the maximum accelerations (using the equations in Table 4, evaluated at the maximum acceleration times established in Table 3) and the value of λ are shown in Table 5. For comparative purposes, the maximum force equations for the case of triangular profiles will also be included.

The values of maximum force with respect to the maximum forces in a triangular profile in terms of saturation are shown in Figs. Figure 7, 8, 9, 10, Fig. 11 for all velocity profiles.

Table 5 Maximum force required for each velocity profile

Velocity profile ramp	Maximum force required
Triangular	$\max(F(\tau)) = F_{I\Delta}(\lambda + 1)$
Linear	$\max(F(\tau)) = F_{I\Delta}\left(\lambda + \frac{1}{(1-\zeta^2)}\right)$
Exponential	$\max(F(\tau)) = F_{I\Delta}\left(\lambda + \frac{5}{(1-\zeta^2)}\right)$
Parabolic	$\max(F(\tau)) = F_{I\Delta}\left(\lambda + \frac{3}{(1-\zeta)(2+\zeta)}\right)$
Sinusoidal	$\max(F(\tau)) = F_{I\Delta}\left(\lambda + \frac{\pi}{2(1-\zeta^2)}\right)$
S-Curve	$\max(F(\tau)) = F_{I\Delta}\left(\lambda + \frac{3}{2(1-\zeta^2)}\right)$

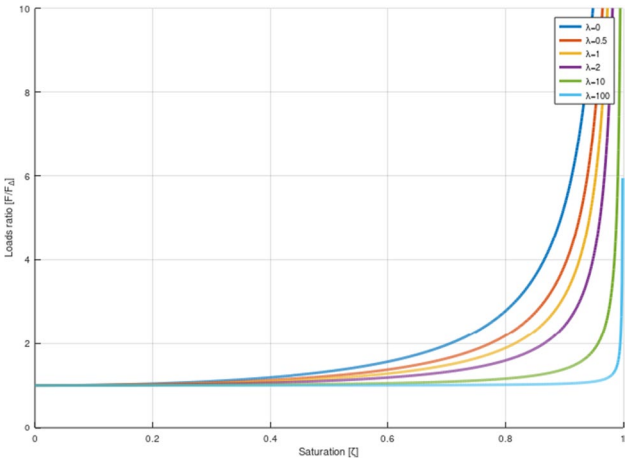

Fig. 7 Influence of saturation on the load ratio in the linear profiles

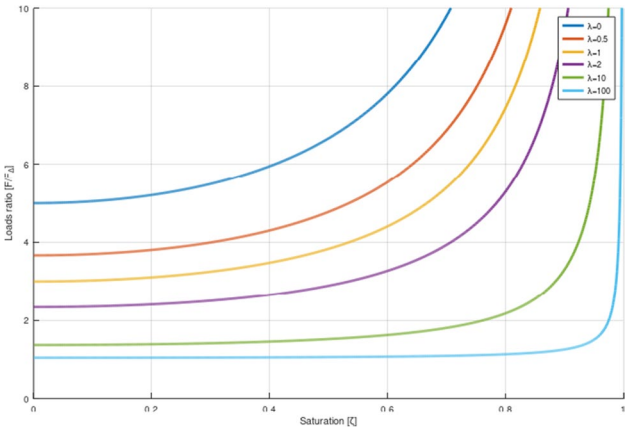

Fig. 8 Influence of saturation on the load ratio in exponential profiles

From the results shown in Figs. Figure 7, 8, 9, 10, Fig. 11, the following conclusions can be drawn regarding the behavior of each velocity profile with reference to the required forces.

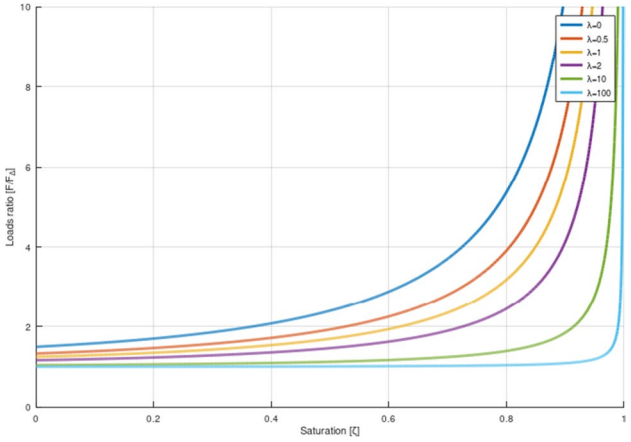

Fig. 9 Influence of saturation on the load ratio in parabolic profiles

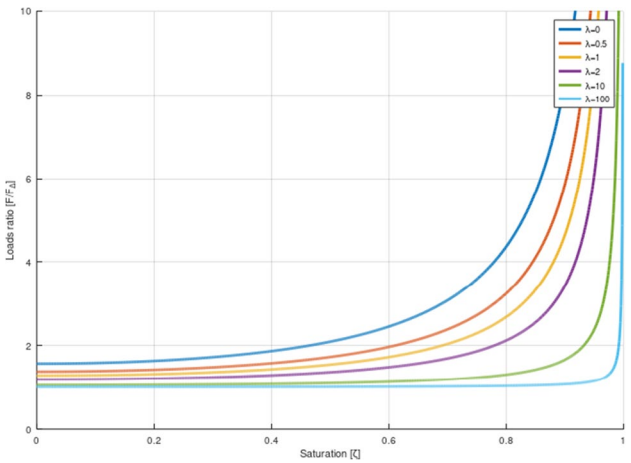

Fig. 10 Influence of saturation on the load ratio in Sinusoidal profiles

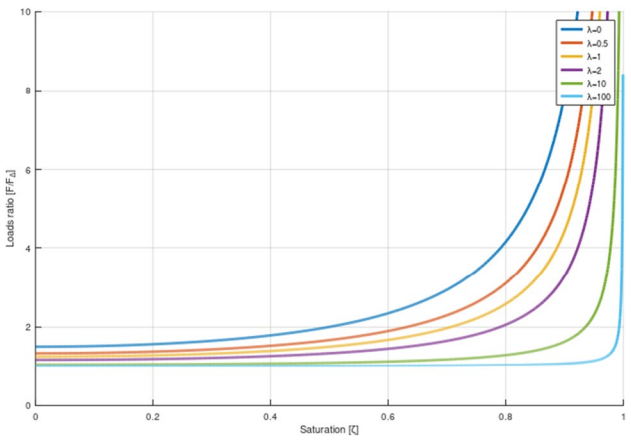

Fig. 11 Influence of saturation on the load ratio in S-curve profiles

- The effect of saturation on force requirements is most significant when the non-inertial loads are small compared to the inertial loads.
- As the non-inertial loads are greater than the inertial ones, the effect of saturation on the total force is less.
- When the saturation value tends to 1, the total force tends to infinity, regardless of the type of profile.
- The effect of saturation on the increase in force is greater in the exponential profiles than in the other profiles.
- The effect of saturation on the force increase is less in the linear profiles than in the other profiles.
- The parabolic, sinusoidal, and s-curve velocity profiles have similar performance in terms of force requirements, being higher than the requirements in the linear profiles but lower than the requirements in exponential profiles.

5 Mechanical power requirements modeling

The instantaneous mechanical power required by a mechanical system is equal to the product of its velocity and its force. The force function, as already explained in the previous section, depends on the ratio of loads and the acceleration function. So, it can be expressed as shown in Eq. 16.

$$P(\tau) = F(\tau)V(\tau) \tag{16}$$

Like the acceleration, the velocity also depends on the instant of time at which it is evaluated, the type of profile, and the saturation, so that it can be expressed as shown in Eq. 17, where $g(\tau, \zeta)$ is a function that varies according to the ramp of the velocity profile.

$$V(\tau) = V_{\Delta} g(\tau, \zeta) \tag{17}$$

Taking as a reference Eqs. 15—17 the power expressed in terms of the inertial power in a triangular profile ($P_{\Delta i}$) and the functions $f(\tau, \zeta)$ and $g(\tau, \zeta)$, as shown in Eq. 18 is obtained:

$$P = ma_{\Delta} V_{\Delta} g(\tau, \zeta)(\lambda + f(\tau, \zeta)) = P_{i\Delta} g(\tau, \zeta)(\lambda + f(\tau, \zeta)) \tag{18}$$

Unlike velocity, acceleration, and force, the maximum value of instantaneous power does not necessarily occur at a specific time since it depends on the value of λ. The instantaneous power equations as a function of dimensionless time are shown in Table 6.

In order to analyse the behavior of mechanical power, the coefficient between the maximum instantaneous power in the profile being analysed and the maximum power reached in a triangular velocity profile will be plotted, for different values of saturation and λ. The maximum power terms were numerically estimated from the equations in Table 6. These results are shown in Fig. 12, 13, 14, 15, Fig. 16.

From the results shown in Figs. Figure 12, 13, 14, 15, Fig. 16, the following conclusions can be drawn regarding the behavior of each velocity profile with reference to the maximum instantaneous mechanical power:

- The maximum power as a function of saturation does not have monotonic behavior in any of the velocity profiles.
- Each profile has a saturation for which the maximum power reaches a minimum value. This saturation depends on the type of ramp and the value of λ.
- In general terms, the lowest maximum instantaneous powers are obtained when using parabolic profiles. In Montalvo et al.'s work [19], the experimental results of comparing the parabolic and linear profiles point to the conclusion that parabolic profiles require lower peak powers, which is consistent with the conclusions obtained in the mathematical modeling of the present work.
- In general terms, the highest maximum instantaneous powers are obtained when using exponential profiles. By comparing the exponential profile with the parabolic profile (when $\lambda = \zeta = 0$), using the equations in Table 6, it can be validated that the maximum power in the exponential profile is 88% higher than that of the parabolic profile.
- The linear, sinusoidal, and S-curve velocity profiles have similar performance in terms of maximum instantaneous power, with the linear profiles having the lowest maximum instantaneous powers within these 3 profiles mentioned.

6 Energy consumption modeling

For this work, the energy consumption model will assume that there are no energy recovery systems such as regenerative braking. The energy required can be calculated by the definition of mechanical work, as shown in Eq. 19.

$$E = \int_0^T \left(\left|F_{Ni} + F_i(t)\right|\right) V(t)dt = \int_0^T |P(\tau)|d\tau \tag{19}$$

The inertial force will be evaluated within an absolute value because during deceleration operations, the drive may be required to impart a negative force to the system, which implies an energy expenditure by the system and not an energy recovery that would be indicated by a negative force. Due to the presence of the absolute value in the integral, it is complex to obtain a general formula for energy consumption. Due to the above, Eq. 20 will be evaluated by numerical integration for particular scenarios. The

Table 6 Instantaneous power as a function of dimensionless time for different types of velocity profiles

Velocity profile ramp	Instantaneous power function	
Triangular	$P(\tau)=\begin{cases} 2P_{i\Delta}\tau(\lambda+1) \\ 2P_{i\Delta}(1-\tau)(\lambda-1) \end{cases}$	$\forall\tau\in\left[0,\frac{(1-\zeta)}{2}\right)$ $\forall\tau\in\left[\frac{(1-\zeta)}{2},1\right]$
Linear	$P(\tau)=\begin{cases} \frac{2P_{i\Delta}\tau}{(1-\zeta^2)}\left(\lambda+\frac{1}{(1-\zeta^2)}\right) \\ \frac{P_{i\Delta}}{(1+\zeta)}\lambda \\ \frac{2P_{i\Delta}(1-\tau)}{(1-\zeta^2)}\left(\lambda-\frac{1}{(1-\zeta^2)}\right) \end{cases}$	$\forall\tau\in\left[0,\frac{(1-\zeta)}{2}\right)$ $\forall\tau\in\left[\frac{(1-\zeta)}{2},\frac{(1+\zeta)}{2}\right)$ $\forall\tau\in\left[\frac{(1-\zeta)}{2},1\right]$
Exponential	$P(\tau)=\begin{cases} \frac{P_{i\Delta}}{(1+\zeta)}\left(1-e^{-\frac{10\tau}{(1-\zeta)}}\right)\left(\lambda+\frac{5}{(1-\zeta^2)}e^{-\frac{10\tau}{(1-\zeta)}}\right) \\ \frac{Pi_{\Delta}}{(1+\zeta)}\lambda \\ \frac{Pi_{\Delta}}{(1+\zeta)}e^{-\frac{5(2\tau-(1+\zeta))}{(1-\zeta)}}\left(\lambda-\frac{5}{(1-\zeta^2)}e^{-\frac{5(2\tau-(1+\zeta))}{(1-\zeta)}}\right) \end{cases}$	$\forall\tau\in\left[0,\frac{(1-\zeta)}{2}\right)$ $\forall\tau\in\left[\frac{(1-\zeta)}{2},\frac{(1+\zeta)}{2}\right)$ $\forall\tau\in\left[\frac{(1-\zeta)}{2},1\right]$
Parabolic	$P(\tau)=\begin{cases} \frac{6P_{i\Delta}\tau((1-\zeta)-\tau)}{(1-\zeta)^2(2+\zeta)}\left(\lambda+\frac{3[(1-\zeta)-2\tau]}{(1-\zeta)^2(2+\zeta)}\right) \\ P_{i\Delta}\left(\frac{3}{2(2+\zeta)}\right)\lambda \\ \frac{6P_{i\Delta}(\tau-\zeta)((1-\zeta)-(\tau-\zeta))}{(1-\zeta)^2(2+\zeta)}\left(\lambda+\frac{3[(1-\zeta)-2(\tau-\zeta)]}{(1-\zeta)^2(2+\zeta)}\right) \end{cases}$	$\forall\tau\in\left[0,\frac{(1-\zeta)}{2}\right)$ $\forall\tau\in\left[\frac{(1-\zeta)}{2},\frac{(1+\zeta)}{2}\right)$ $\forall\tau\in\left[\frac{(1-\zeta)}{2},1\right]$
Sinusoidal	$P(\tau)=\begin{cases} \frac{P_{i\Delta}}{2(1+\zeta)}\left(1-\cos\left(\frac{2\pi\tau}{(1-\zeta)}\right)\right)\left(\lambda+\frac{1}{2(1-\zeta^2)}\left(\pi sen\left(\frac{2\pi\tau}{(1-\zeta)}\right)\right)\right) \\ \frac{P_{i\Delta}\lambda}{(1+\zeta)} \\ \frac{P_{i\Delta}}{2(1+\zeta)}\left(1-\cos\left(\frac{2\pi(\tau-\zeta)}{(1-\zeta)}\right)\right)\left(\lambda+\frac{1}{2(1-\zeta^2)}\left(\pi sen\left(\frac{2\pi(\tau-\zeta)}{(1-\zeta)}\right)\right)\right) \end{cases}$	$\forall\tau\in\left[0,\frac{(1-\zeta)}{2}\right)$ $\forall\tau\in\left[\frac{(1-\zeta)}{2},\frac{(1+\zeta)}{2}\right)$ $\forall\tau\in\left[\frac{(1-\zeta)}{2},1\right]$
S-Curve	$P(\tau)=\begin{cases} \frac{4P_{i\Delta}}{(1+\zeta)}\left(\frac{3\tau^2}{(1-\zeta)^2}-\frac{4\tau^3}{(1-\zeta)^3}\right)\left(\lambda+\frac{12\tau}{(1+\zeta)}\left(\frac{(1-\zeta)-2\tau}{(1-\zeta)^3}\right)\right) \\ \frac{P_{i\Delta}\lambda}{(1+\zeta)} \\ \frac{4P_{i\Delta}}{(1-\zeta)^3(1+\zeta)}(1-\tau)^2(4\tau-3\zeta-1)\left(\lambda+\frac{12}{(1+\zeta)}\left(\frac{(1-\zeta)^2-3(1-\zeta)(\tau-\zeta)+2(\tau-\zeta)^2}{(1-\zeta)^3}\right)\right) \end{cases}$	$\forall\tau\in\left[0,\frac{(1-\zeta)}{2}\right)$ $\forall\tau\in\left[\frac{(1-\zeta)}{2},\frac{(1+\zeta)}{2}\right)$ $\forall\tau\in\left[\frac{(1-\zeta)}{2},1\right]$

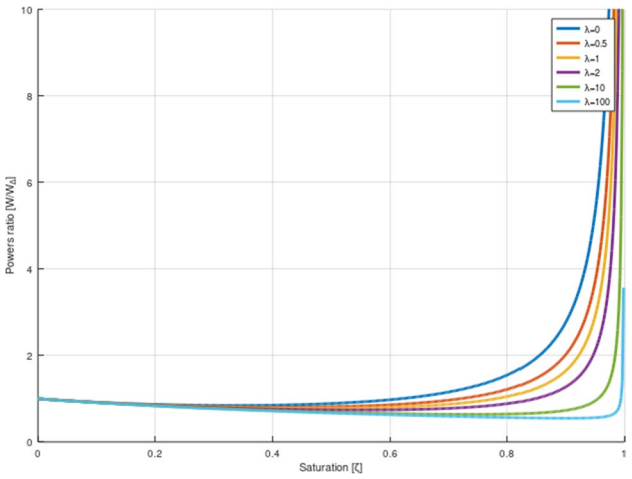

Fig. 12 Influence of saturation on the ratio of mechanical powers in the linear profile

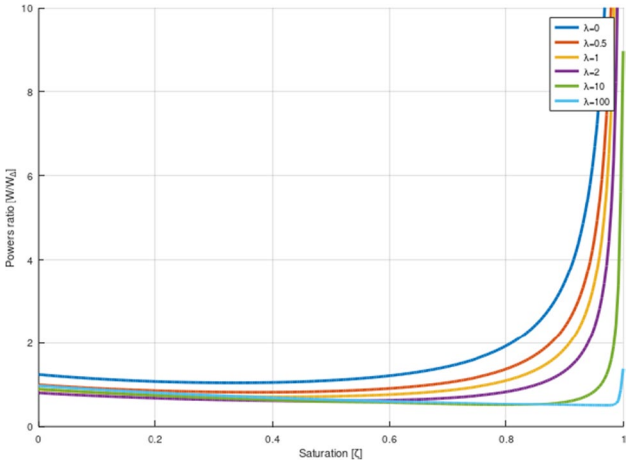

Fig. 13 Influence of saturation on the ratio of mechanical powers in the exponential profile

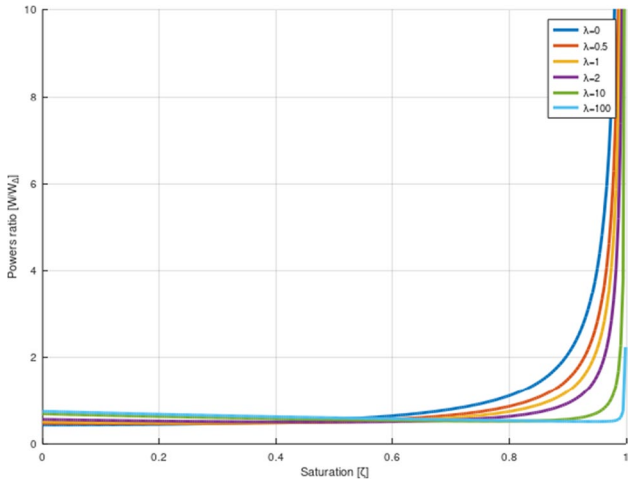

Fig. 14 Influence of saturation on the ratio of mechanical powers in the parabolic profile

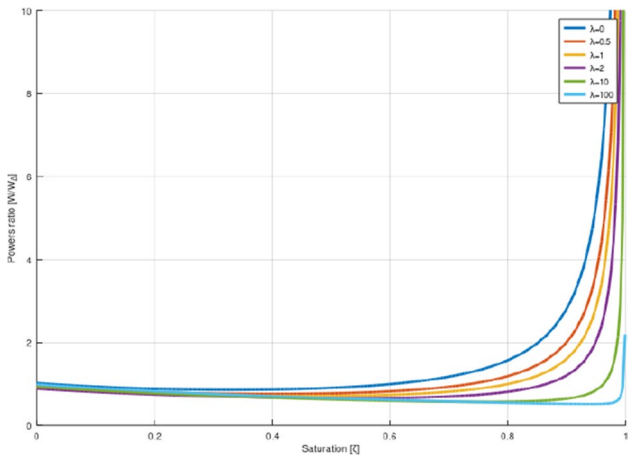

Fig. 15 Influence of saturation on the ratio of mechanical powers in the sinusoidal profile

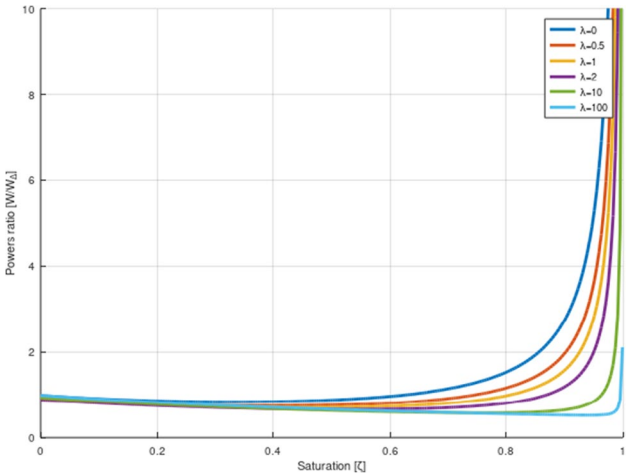

Fig. 16 Influence of saturation on the ratio of mechanical powers in the S-curve profile

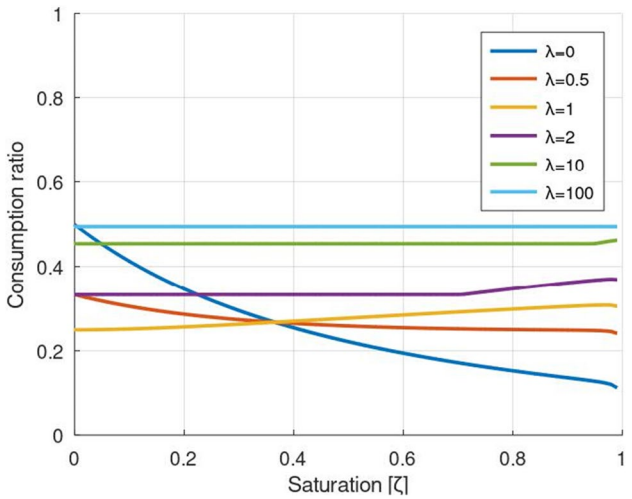

Fig. 17 Influence of saturation on the ratio of energy consumption in the linear profile

purpose of Eq. 20 is to adimensionalize the power before integration, taking as a reference the maximum triangular power for the specific value of λ for each scenario.

$$E = \int_0^T \frac{|P(\tau)|}{\max(P_\Delta(\tau))} d\tau \tag{20}$$

In order to analyse the behavior of energy consumption, the coefficient between the energy consumption in the profile being analysed and the energy consumed in a triangular profile for different values of ζ and λ will be plotted. These results are shown in Figs. Figure 17–Fig. 21. For $(0 \leq \zeta < 1)$ which comprises the range of values between which saturation can be found, the consumption for linear, exponential, sinusoidal, and s-curve profiles is almost identical, although the consumption equation for exponential profiles is different.

From the results shown in Figs. Figure 17, 18, 19, 20, Fig. 21 the following conclusions can be drawn regarding the behavior of each velocity profile with reference to energy consumption:

- The higher the saturation, the lower the energy consumption. This is because the displacement at which the inertial forces do mechanical work decreases. For low values of λ, energy consumption tends to decrease with saturation, while for medium values (0.5–2, depending on the profile), energy consumption tends to increase with saturation.

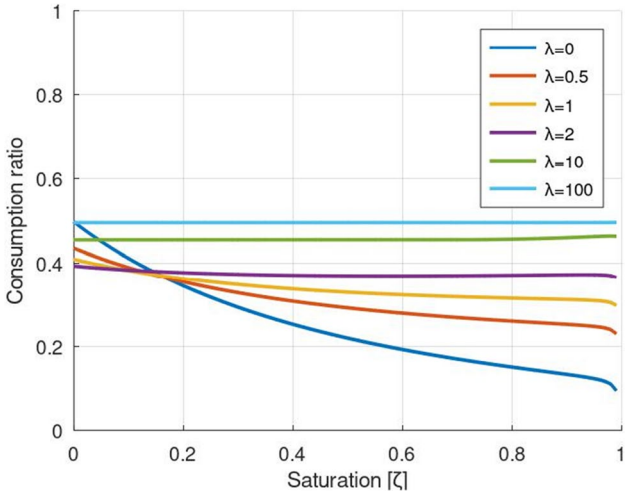

Fig. 18 Influence of saturation on the ratio of energy consumption in the exponential profile

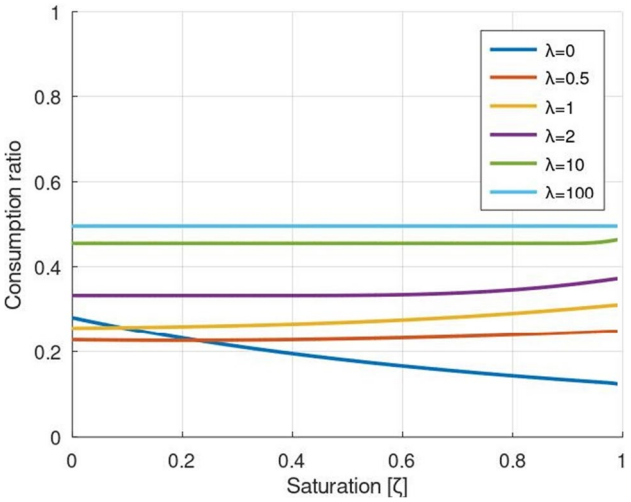

Fig. 19 Influence of saturation on the ratio of energy consumption in the parabolic profile

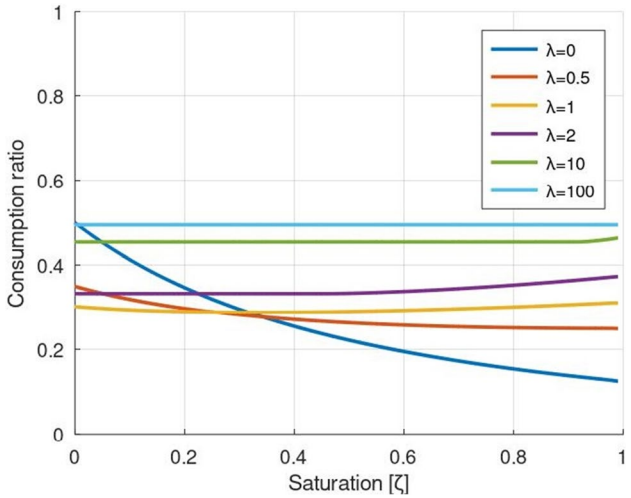

Fig. 20 Influence of saturation on the ratio of energy consumption in the sinusoidal profile

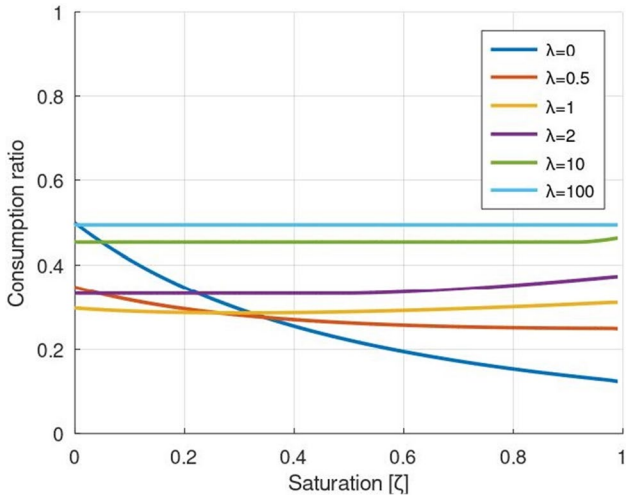

Fig. 21 Influence of saturation on the ratio of energy consumption in the S-curve profile

- When λ tends to be large, the effect of saturation on energy consumption tends to decrease.
- In general terms, parabolic velocity profiles lead to the lowest energy consumption. This conclusion is supported experimentally in the work of Montalvo et al. [19], where for the analysed case study, it was validated that the energy consumption of the parabolic velocity profiles is lower than the consumption presented in the linear profiles.
- Velocity profiles with linear, sinusoidal, and s-curve ramps have similar energy consumptions. The similarity in energy consumption of the linear, s-curve, and sinusoidal profiles is consistent with the experimental studies performed by Carabin et al. [20].
- In general terms, the highest energy consumption is obtained when using exponential profiles.

7 Guidelines for velocity profile selection

Considering the results obtained in the previous sections, the following guidelines are proposed for the selection of the appropriate velocity profile type:

- In the absence of any specific constraints or requirements, linear ramp profiles will be used. This is because these profiles are the simplest to calculate, easy to control, and generate the lowest accelerations, consequently resulting in lower loads for the motor.
- In cases where it is necessary to minimize vibrations associated with jerking, smooth curve profiles should be employed, such as parabolic, sinusoidal, or S-curve profiles. To take advantage of this characteristic in these types of profiles, saturation should be set to zero, as otherwise, discontinuities will occur. In this scenario, it is suggested to use sinusoidal or S-curve profiles over parabolic profiles, as the former minimize jerking.
- If it is necessary to minimize the receiver's velocity, it is advisable to use velocity profiles with parabolic ramps.
- In cases where the goal is to minimize energy or nominal power, it is suggested to use the parabolic profile if non-inertial loads are less than or equal to inertial loads ($\lambda \leq 1$). This is because parabolic profiles result in the lowest energy consumption and lower maximum power over most of the saturation range when $\lambda \leq 1$. Otherwise, the linear velocity profile should be chosen, as it generates similar consumption and power requirements to the parabolic profile for the range of $\lambda > 1$.
- The use of profiles with exponential ramps is discouraged, as the requirements for mechanical power and torque are higher for motions performed with these profiles compared to their counterparts. They do not offer any additional benefits in terms of kinematics or kinetics that justify their selection.

The advantages and disadvantages of each profile are shown in Table 7 using a scoring system, with one star being poor performance with respect to the variable of interest and three stars being good performance with respect to the variable of interest.

Table 7 Comparative summary of velocity profiles

Velocity pramp	Linear	Exponential	Parabolic	Sinusoidal/ S-curve
Maximum velocity	★★	★★	★★★	★★
Maximum acceleration	★★★	★	★★	★★
Maximum force	★★★	★	★★	★★
Maximum mechanical power	★★★	★	★★★	★★
Energy consumption	★★	★★	★★★	★★
Jerk	★	★	★★	★★★

8 Conclusions

A novel methodology for the correct selection of velocity profiles to optimize 1 DOF manipulator performance minimizes variables such as velocity, acceleration, jerk, forces, mechanical power, or energy consumption according to the design requirements.

Initially, mathematical models were developed to estimate the values of velocity, acceleration, forces, peak power, and energy consumption for different types of velocity profiles, different saturation values, and external load conditions.

From a kinematic point of view, the selection of the profile type can increase the maximum velocity by up to 33.3% (the minimum value being that of the parabolic profiles) and the acceleration by more than 400%, depending on the saturation used (the minimum value being that of the linear profiles and the maximum value being that of the exponential profiles).

On the other hand, it was also shown that failure to use the methodology could result in significantly high increases in peak forces, rated power, and energy consumption, which will ultimately impact the initial and operating costs of the system and the sustainability of the design. Analogous to the speed, the selection of the speed profile can increase the forces required by the drive system by up to 400% (the minimum value being that of the linear profiles and the maximum value being that of the exponential profiles) and the maximum power required by more than 88%, which can increase depending on the saturation chosen (the minimum value being that of the parabolic profiles and the maximum value being that of the exponential profiles).

For the case of energy consumption, it was estimated that depending on the value of ζ and λ, linear, exponential, sinusoidal, and s-curve profiles can generate consumptions up to 77% higher than parabolic profiles. Although the actual energy consumption figures will depend on other factors, such as motor parameters and speed control, the decrease in energy consumption when using parabolic profiles instead of linear profiles has been experimentally validated.

Finally, a series of guidelines were established to select the most appropriate speed profile according to the load regime and the designer's specific desires, which will contribute to improving their performance and reducing the initial and operating costs of the manipulator during its lifetime, as well as minimizing its energy and environmental impact.

The superiority of this methodology lies in the following aspects:

- It simultaneously considers multiple velocity profiles instead of focusing on a single profile, allowing for comparisons with trapezoidal profiles, which are the most commonly used.

- It does not require the pre-selection of motors to implement the methodology.
- It simultaneously analyses several variables of interest, such as velocity, acceleration, force, mechanical power, and energy consumption, obtaining significant reductions in the values of performance indicators.
- It incorporates the saturation of the velocity profile as a variable of interest in the mathematical modeling.
- It includes non-inertial forces in the models.

Author contribution Camilo Gonzalez: Conceptualization, Formal analysis, Visualization, Writing— original draft, Writing—review & editing. Heriberto Maury: Supervision, Formal analysis, Writing—review & editing Leidy Mora: Visualization, Writing—original draft.

Funding Open Access funding provided by Colombia Consortium

Declarations

Competing interests The authors declare that they have no competing interests.

References

1. Bechar A, Vigneault C (2017) Agricultural robots for field operations. Part 2: operations and systems. Biosyst Eng 153:110–128. https://doi.org/10.1016/j.biosystemseng.2016.11.004
2. Mu L, Cui G, Liu Y et al (2020) Design and simulation of an integrated end-effector for picking kiwifruit by robot. Inf Process Agric 7:58–71. https://doi.org/10.1016/j.inpa.2019.05.004
3. Huynh HN, Assadi H, Rivière-Lorphèvre E, et al (2020) Modelling the dynamics of industrial robots for milling operations. Robot Comput Integr Manuf 61. https://doi.org/10.1016/j.rcim.2019.101852
4. Urhal P, Weightman A, Diver C, Bartolo P (2019) Robot assisted additive manufacturing: a review. Robot Comput Integr Manuf 59:335–345. https://doi.org/10.1016/j.rcim.2019.05.005
5. Furtado LFF, Villani E, Trabasso LG, Sutério R (2017) A method to improve the use of 6-dof robots as machine tools. Int J Adv Manuf Technol 92:2487–2502. https://doi.org/10.1007/s00170-017-0336-8
6. Lai CY, Villacis Chavez DE, Ding S (2018) Transformable parallel-serial manipulator for robotic machining. Int J Adv Manuf Technol 97:2987–2996. https://doi.org/10.1007/s00170-018-2170-z
7. Ghadiri Nejad M, Shavarani SM, Güden H, Barenji RV (2019) Process sequencing for a pick-and-place robot in a real-life flexible robotic cell. Int J Adv Manuf Technol 103:3613–3627. https://doi.org/10.1007/s00170-019-03739-6
8. Bi ZM, Luo C, Miao Z et al (2021) Safety assurance mechanisms of collaborative robotic systems in manufacturing. Robot Comput Integr Manuf 67:102022. https://doi.org/10.1016/j.rcim.2020.102022
9. Daneshmand M, Bilici O, Bolotnikova A, Anbarjafari G (2017) Medical robots with potential applications in participatory and opportunistic remote sensing: a review. Rob Auton Syst 95:160–180. https://doi.org/10.1016/j.robot.2017.06.009
10. Alexovič M, Dotsikas Y, Bober P, Sabo J (2018) Achievements in robotic automation of solvent extraction and related approaches for bioanalysis of pharmaceuticals. J Chromatogr B 1092:402–421. https://doi.org/10.1016/j.jchromb.2018.06.037
11. Boscariol P, Richiedei D (2019) Energy-efficient design of multipoint trajectories for Cartesian robots. Int J Adv Manuf Technol 102:1853–1870. https://doi.org/10.1007/s00170-018-03234-4
12. Atakuru T, Samur E (2018) A robotic gripper for picking up two objects simultaneously. Mech Mach Theory 121:1339–1351. https://doi.org/10.1016/j.mechmachtheory.2017.10.027
13. Senatore A, Ventura G (2022) EOD robot mechatronic modelling and trajectory optimization through Chebyshev polynomials. 2022 25th International Conference on Mechatronics Technology (ICMT) 1–5. https://doi.org/10.1109/ICMT56556.2022.9997625
14. Van Oosterwyck N, Vanbecelaere F, Knaepkens F et al (2022) Energy optimal point-to-point motion profile optimization. Mech Based Des Struct Mach. https://doi.org/10.1080/15397734.2022.2106241
15. Chen H, Mu H, Zhu Y (2016) Real-time generation of trapezoidal velocity profile for minimum energy consumption and zero residual vibration in servomotor systems. Am Control Conf (ACC) 2016:2223–2228. https://doi.org/10.1109/ACC.2016.7525248
16. García J, Martinez M, Rodriguez J, Cruz E (2017) Assessment of jerk performance S-curve and trapezoidal velocity profiles. 2017 XIII International Engineering Congress (CONIIN) : Universidad Autónoma de Querétaro, Santiago de Queretáro, Mexico : from 2017–05–15 to 2017–05–19
17. Heo HJ, Son Y, Kim JM (2019) A trapezoidal velocity profile generator for position control using a feedback strategy. Energies (Basel) 12. https://doi.org/10.3390/en12071222
18. Yu Z, Han C, Haihua M (2015) A novel approach of tuning trapezoidal velocity profile for energy saving in servomotor systems. 2015 34th Chinese Control Conference (CCC) 4412–4417. https://doi.org/10.1109/ChiCC.2015.7260323
19. Montalvo V, Estévez-Bén AA, Rodríguez-Reséndiz J et al (2020) FPGA-based architecture for sensing power consumption on parabolic and trapezoidal motion profiles. Electronics (Switzerland) 9:1–22. https://doi.org/10.3390/electronics9081301
20. Carabin G, Vidoni R (2021) Energy-saving optimization method for point-to-point trajectories planned via standard primitives in 1-DoF mechatronic systems. Int J Adv Manuf Technol 116:331–344. https://doi.org/10.1007/s00170-021-07277-y
21. Fang Y, Qi J, Hu J et al (2020) An approach for jerk-continuous trajectory generation of robotic manipulators with kinematical constraints. Mech Mach Theory 153. https://doi.org/10.1016/j.mechmachtheory.2020.103957
22. Halinga MS, Nyobuya HJ, Uchiyama N (2023) Generation and experimental verification of time and energy optimal coverage motion for industrial machines using a modified S-curve

trajectory. Int J Adv Manuf Technol 125:3593–3605. https://doi.org/10.1007/s00170-023-10912-5
23. Assad F, Rushforth E, Ahmad M et al (2018) An approach of optimising S-curve trajectory for a better energy consumption. 2018 IEEE 14th International Conference on Automation Science and Engineering (CASE) 98–103. https://doi.org/10.1109/COASE.2018.8560587
24. Zhang Y, Yang H, Yang D et al (2020) Polynomial profile optimization method of a magnetic petal-shaped capsule robot. Mechatronics 65. https://doi.org/10.1016/j.mechatronics.2019.102309
25. Siripala PJ, Sekercioglu YA (2013) A generalised solution for generating stepper motor speed profiles in real time. Mechatronics 23:541–547. https://doi.org/10.1016/j.mechatronics.2013.04.004
26. Olier CAG, Ramírez HEM, Manotas VJP (2023) A novel methodology focused on the selection of the movement strategy to minimize power and energy consumption of drive systems for manufacturing robots in pick-and-place applications. Int J Adv Manuf Technol 125:4309–4319. https://doi.org/10.1007/s00170-022-10572-x
27. Izumi T, Li Z, Zhou H (2008) A reduction ratio for minimizing dissipated energy in a mechatronic system with a gear train. Mechatronics 18:529–535. https://doi.org/10.1016/j.mechatronics.2008.07.001
28. Roos F, Johansson H, Wikander J (2006) Optimal selection of motor and gearhead in mechatronic applications. Mechatronics 16:63–72. https://doi.org/10.1016/j.mechatronics.2005.08.001
29. Park JS (1996) Motion profile planning of repetitive point-to-point control for maximum energy conversion efficiency under acceleration conditions. Mechatronics 6:649–663. https://doi.org/10.1016/0957-4158(96)00012-8
30. González Coneo J, Quiroz Mariano V, Maury H et al (2006) Aplicación de metodos para el diseño y selección de accionamientos rápidos. Ing Desarro 20:78–171
31. Cusimano G (2007) Optimization of the choice of the system electric drive-device-transmission for mechatronic applications. Mech Mach Theory 42:48–65. https://doi.org/10.1016/j.mechmachtheory.2006.02.003
32. Cusimano G (2005) Generalization of a method for the selection of drive systems and transmissions under dynamic loads. Mech Mach Theory 40:530–558. https://doi.org/10.1016/j.mechmachtheory.2004.12.002
33. Gerbaud L, Bigeon J, Champenois G (1993) Expert system bases to automate selection of drive structures. In: IECON Proceedings (Industrial Electronics Conference). Publ by IEEE, pp 360–365. https://doi.org/10.1109/IECON.1993.339052
34. Maury Ramirez H, Domènech Mestres C, Riba Romeva C et al (2003) Comparative analysis of triangular and trapezoidal speed diagrams as speed diagrams as strategies for rapid movements. In: 7th International Research/Expert Conference "Trends in the Development of Machinery and Associated Technology" TMT 2003, Lloret de Mar, Barcelona, Spain
35. Stojanovic V (2023) Fault-tolerant control of a hydraulic servo actuator via adaptive dynamic programming. Math Model Control 3:181–191. https://doi.org/10.3934/mmc.2023016
36. Zhang H (2022) Adaptive fuzzy controller design for uncertain robotic manipulators subject to nonlinear dead zone inputs. Comput Intell Neurosci 2022. https://doi.org/10.1155/2022/9173249
37. Azizi Y, Yazdizadeh A (2019) Passivity-based adaptive control of a 2-DOF serial robot manipulator with temperature dependent joint frictions. Int J Adapt Control Signal Process 33:512–526. https://doi.org/10.1002/acs.2968
38. Golestani M, Chhabra R, Esmaeilzadeh M (2023) Finite-time nonlinear H∞Control of robot manipulators with prescribed performance. IEEE Control Syst Lett 7:1363–1368. https://doi.org/10.1109/LCSYS.2023.3241137
39. Rao P, Chakraverty S, Roy D (2024) Oscillation characteristics of single-link flexible manipulator using design parameters in fuzzy domain. J Vib Eng Technol. https://doi.org/10.1007/s42417-024-01410-3
40. Ali A (2017) Fuzzy control for a two-DOF manipulator system. Am J Artif Intell 1. https://doi.org/10.11648/j.ajai.20170101.17
41. Urrea C, Kern J, Alvarado J (2020) Design and evaluation of a new fuzzy control algorithm applied to a manipulator robot. Appl Sci (Switzerland) 10:1–21. https://doi.org/10.3390/app10217482
42. Puphal T, Probst M, Li Y et al (2018) Optimization of velocity ramps with survival analysis for intersection merge-ins. IEEE Intell Veh Symp (IV) 2018:1704–1710. https://doi.org/10.1109/IVS.2018.8500667
43. Rymansaib Z, Iravani P, Sahinkaya MN (2013) Exponential trajectory generation for point to point motions. IEEE/ASME Int Conf Adv Intell Mechatron 2013:906–911. https://doi.org/10.1109/AIM.2013.6584209
44. Wang G, Xu F, Zhou K, Pang Z (2022) S-Velocity profile of industrial robot based on NURBS curve and slerp interpolation. Processes 10. https://doi.org/10.3390/pr10112195
45. Boscariol P, Richiedei D (2018) Spline-based energy-optimal trajectory planning for functionally redundant robots. 2018 14th IEEE/ASME International Conference on Mechatronic and Embedded Systems and Applications (MESA). https://doi.org/10.1109/MESA.2018.8449155
46. Fang Y, Hu J, Liu W et al (2019) Smooth and time-optimal S-curve trajectory planning for automated robots and machines. Mech Mach Theory 137:127–153. https://doi.org/10.1016/j.mechmachtheory.2019.03.019
47. Halinga MS, Nyobuya HJ, Uchiyama N (2023) Generation of time and energy optimal coverage motion for industrial machines using a modified S-curve trajectory. 2023 IEEE/SICE International Symposium on System Integration (SII) 1–6.https://doi.org/10.1109/SII55687.2023.10039252